J. Mol. Model. **2000**, *6*, 16 – 25

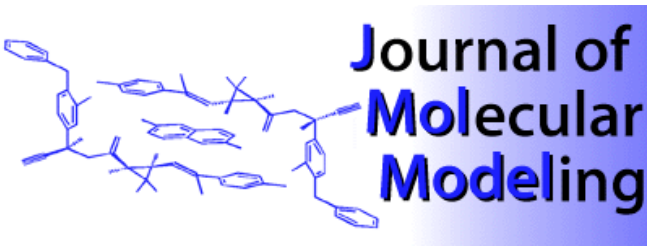

FULL PAPER

Structural Insights Into NMDA Ionotropic Glutamate Receptors *via* Molecular Modelling

Kamaldeep K. Chohan[1], Z. Galen Wo[2], Robert E. Oswald[2], and Michael J. Sutcliffe[1]

[1]Department of Chemistry, University of Leicester, Leicester, LE1 7RH, United Kingdom. Tel.: +44-116 252 3601; Fax: +44-116 252 3789. E-mail: sjm@le.ac.uk

[2]Department of Molecular Medicine, Cornell University, Ithaca, NY 14853, USA

Received: 19 November 1999/ Accepted: 22 December 1999/ Published: 17 January 2000

Abstract Structural models have been produced for the agonist binding and transmembrane domains of two NMDA ionotropic glutamate receptors: homomeric NMDA-R2C and heteromeric NMDA-R1/R2C. These models—produced using homology modelling techniques in conjunction with distance restraints derived from the accessibility of substituted cysteines—have aided our understanding of **(1)** ligand selectivity and **(2)** channel activity. The model of the agonist binding domain of NMDA-R2C indicates that T691 forms an essential hydrogen bond with glutamate ligand. This interaction is absent in the NMDA-R1 model—where a valine replaces the threonine—explaining why NMDA-R1 binds glycine rather than glutamate. For the transmembrane region, the models suggest that a number of positive residues, located in the cytoplasmic loop between the M1 and M2 segments, create a large electrostatic energy barrier that could explain why homomeric NMDA-R2C channels are non-functional. Introducing NMDA-R1 to form heteromeric NMDA-R1/R2C channels is predicted to rescue channel activity because the corresponding region in NMDA-R1 contains negative residues that more than compensate for the electrostatic energy barrier in NMDA-R2C. These studies suggest that replacing the positively charged region in the M1-M2 loop of NMDA-R2C with the corresponding negatively charged region of NMDA-R1 could transform NMDA-R2C into a functional homomeric channel.

Keywords Agonist binding, Selectivity, Cation channel

Introduction

Glutamate receptors are large multisubunit transmembrane proteins that are vital components of the central nervous system. Both G protein-linked (metabotropic) glutamate receptors and glutamate receptors with intrinsic cation channels (ionotropic, iGluRs) are found in vertebrate neuronal cells. The ionotropic receptors bind glutamate (and glycine in the case of NMDA-R1 receptors), which produces a conformational change in the extracellular portion of the protein (see, *e.g.*, [1]) that results in the opening of an ion channel. These receptors mediate fast synaptic transmission and have been implicated in a number of normal processes [2] such as memory and learning, and in pathological processes such as epilepsy, Parkinson's disease, ischemic stroke and AIDS. A number of proteins have been cloned that com-

Correspondence to: M. J. Sutcliffe

prise subunits of intact iGluRs. These are classified according to the other subunits with which they associate and the specific agonist by which they can be activated (see, *e.g.*, [3] for a review): **(1)** a-amino-3-hydroxy-5-methyl-4-isoxazolepropionate (AMPA) receptors (GluR1 to 4), **(2)** kainate receptors (GluR5 to 7 and KA1 to 2), and **(3)** N-methyl-D-aspartate (NMDA) receptors (NMDA-R1 to NMDA-R2D).

Based on homology with bacterial amino acid binding proteins and bacterial and eukaryotic potassium channels, iGluRs are proposed to have a modular structure, consisting of [4]: **(i)** An extracellular domain, evolved from 2 different classes of bacterial proteins, with the N-terminal half homologous to the leucine, isoleucine, valine-binding protein (LIVBP) and the C-terminal half homologous to the lysine, arginine, ornithine-binding protein (LAOBP) and glutamine binding protein [5,6]. The agonist binds to this C-terminal subdomain. **(ii)** A transmembrane region that consists of two membrane spanning regions and a reentrant loop [7-9]. Based on sequence homologies, this region is thought to have a similar topology to K^+ channels [10,11]. **(iii)** a cytoplasmic C-terminal domain that is highly variable and that is involved in cytoskeletal interactions, and may have a regulatory role [12-14].

The work presented here focuses on NMDA receptor structure and function. In nature, the NMDA receptors exist as heteromeric proteins, containing both NMDA-R1 and NMDA-R2 subunits (see, *e.g.*, [3]). NMDA-R1 receptors were originally cloned based on their ability to form homomeric functional channels in *Xenopus* oocytes [15]. However, subsequent work suggests that NMDA-R1 actually forms a heteromeric channel with an endogenous *Xenopus* NMDA receptor subunit [16]. Homomeric channels of the NMDA-R2 subfamily do not form functional channels [17]. Molecular models of both the pore forming region and agonist binding domain of homomeric NMDA-R2C and heteromeric NMDA-R1/R2C channels have been produced. The models provide an explanation for the lack of functional ion channel activity for homomeric NMDA-R2 receptors and provide insights into the differential interactions of these two subunits with glycine and glutamate [18-20]. This study extends our earlier work [21], performed before the crystal structures of the agonist binding domain of GluR2 [22] and the KcsA K^+ channel [23] were available.

Methods

The molecular modelling was performed using methods described previously [21,24,25]. In brief, each subunit is divided into domains, which are modelled independently. The results are then combined to give insight into the intact receptor. Our studies are centred on modelling the transmembrane and agonist binding domains of NMDA-R2C (as a homomeric channel to investigate how this non-functional channel could be modified to become functional) and NMDA-R1 (as a heteromeric NMDA-R1/R2C channel). NMDA-R2C was chosen in preference to other NMDA-R2 subunits because experimental data for the exposure of residues to the ion conduction pathway are available for heteromeric NMDA-R1/R2C channels.

Transmembrane domain

The amino acid sequences corresponding to the transmembrane domains of NMDA-R1, NMDA-R2A, NMDA-R2B, NMDA-R2C and NMDA-R2D receptors were aligned using ClustalW [26] (Figure 1). Given the previously suggested homology between the M1-M2-M3 region of the channels and the S5-H5-S6 (or M1-P-M2) region of K^+ channels [10,11], the crystal structure [23] of the KcsA K^+ channel from *Streptomyces lividans* (PDB [27] accession code: 1BL8) was used as the only appropriate structural template for building the models (sequence identity of 9 % and 14 % with NMDA-R2C and NMDAR1/R2C, respectively). The amino acid sequence of KcsA was aligned against the previously determined alignment of the NMDA receptor sequences using ClustalW, the latter being treated as a "profile" (*i.e.* the NMDA sequences were fixed with respect to each other and the KcsA sequence appended to this alignment). In doing so it was ensured that the K^+ channel signature sequence (GYG on KcsA) aligned with the corresponding regions on the NMDA receptors (*i.e.* ^{618}GIG^{620} and ^{617}SVP^{619} [positions *N+2* to *N+4*] for NMDA-R1 and NMDA-R2C, respectively). For the NMDA receptors, the secondary structure was predicted using the consensus secondary structure prediction server Jpred [28]. The alignment was adjusted manually using Cameleon (Oxford Molecular Ltd., Oxford, UK) to optimise the correlation of secondary structure between all sequences, continuing to treat the sequences of the NMDA receptors as a "profile". However, it should be stressed that, given the low sequence homology between the KcsA template and the structures being modelled, there is some ambiguity in the alignment, particularly in those regions outside M1, M2 and M3.

The program Modeller [29] was used, in conjunction with distance restraints derived from the accessibility of substituted cysteines and symmetry restraints (to give a tetramer), to produce a set of 10 models for homomeric NMDA-R2C receptors. Modeller uses simulated annealing, followed by energy minimisation, to refine the models in conjunction with a combination of user-defined restraints and restraints derived from the structure of the template. The distance restraints were derived from studies reporting channel block resulting from scanning cysteine mutagenesis followed by application of methanethiosulphonate (MTS)-based thiol reagents, from both the extracellular and cytoplasmic side, to a heteromeric NMDA-R1/NMDAR-2C channel [30]. If block was observed from the extracellular or intracellular side (but not both), then the maximum gamma atom–gamma atom (*e.g.* Cγ–Cγ) distance across the pore at that position was set at 20 Å for all such residue positions (given that MTS reagents covalently bind to the Sγ atom of cysteine, and assuming that the length of the MTS reagents used is ~10 Å), apart from glycines, which were set to a maximum Cα–Cα cross-pore distance of

24 Å. If block occurred from both sides this implied that the residue was accessible from both sides of the membrane and therefore is part of the selectivity filter (the narrowest part of the channel). For such positions the maximum distance across the pore was set at 10 Å for all residues (a conservative estimate of the gamma atom-gamma atom distance across the narrowest part of the pore), apart from 14 Å for glycines. When there was no block, no restraints were applied because

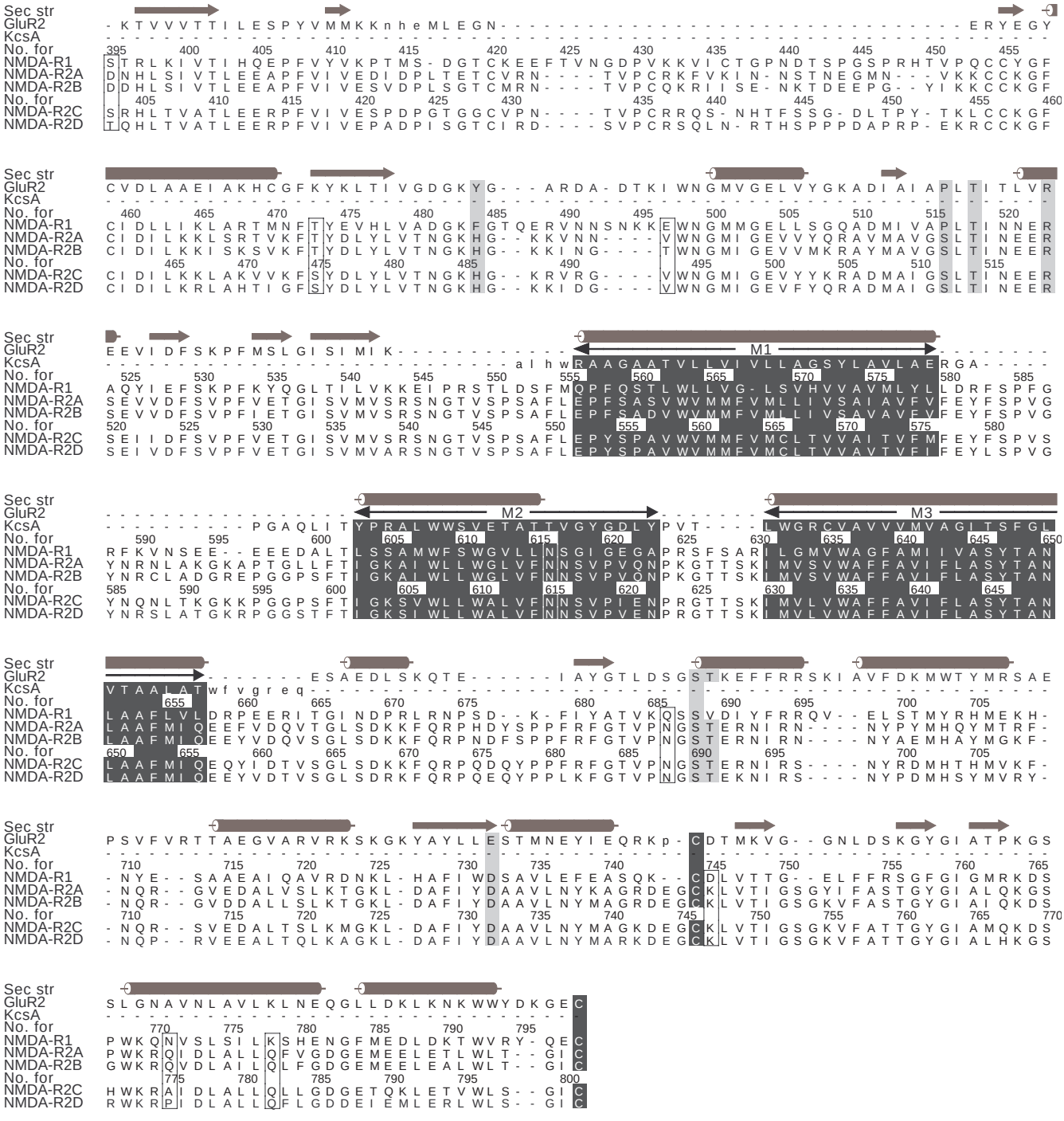

Figure 1 *Sequence alignment of the NMDA receptors and the structural templates used for modelling. The crystallographically-determined secondary structure is shown, as are the consensus glycosylation sites (vertical boxes), ligand binding residues (grey background), the position of the conserved disulphide bridge (black background) and the Q/R/N site (in M2; white box). Template residues shown in lower case were not used in the modelling. (Generated using Alscript [56])*

Table 1 *Stereochemical quality of the models as determined from PROCHECK*

Protein	Residues in "most favoured" regions (%)	G-factor [a]
Transmembrane domain		
KcsA (template)	75	0.1
NMDA-R2C	62	-0.5
NMDA-R1/R2C	64	-0.6
NMDA-R2C mutant [b]	61	-0.5
Agonist binding domain		
GluR2 (template)	93	0.3
NMDA-R1	84	-0.2
NMDA-R2C	86	-0.1

[a] Ideally values should be > -0.5. Values < -1.0 need further investigation.
[b] "NMDA-R2C mutant" refers to homomeric (^{591}KGKKPGGP^{598}) NMDA-R2C (EEEEED)

interpretation was ambiguous—the residue could be buried but still relatively close to the centre of the pore. A C_4 symmetry restraint was applied for the homomeric channels because **(1)** the crystal structure of the KcsA K^+ channel is tetrameric, and **(2)** it has been suggested that iGluRs are also tetrameric [31-33]. However, experimental determination of the stoichiometry remains somewhat ambiguous, and some studies suggest that the iGluRs are pentameric [34]. Any consistent stereochemical violations across the set of models were removed by manual adjustment of the sequence alignment within Cameleon (again treating the NMDA receptor sequences as a "profile"). In adjusting the alignment it was ensured that amino acid insertions and/or deletions were not introduced into the secondary structural elements of the crystallographically-determined secondary structure of KcsA. The lowest energy model was analysed using interactive molecular graphics (InsightII; MSI, San Diego, CA), compared with previous models [21], mutagenesis data [35] and polyamine binding studies [36,37].

This modelling procedure was repeated for: (i) a NMDA-R1/NMDA-R2C heteromeric channel (here a C_2, rather than C_4, symmetry restraint was applied), and (ii) a homomeric NMDA-R2C mutant where the residues ^{591}KGKKPGGP^{598} in the loop between M1 and M2 were replaced by the corresponding region ^{594}EEEEED^{599} on NMDA-R1. An indication of the stereochemical quality of the models is given in Table 1. Electrostatic calculations were performed on all models using the program Delphi [38] (including electrostatic focussing in which the protein occupied initially 20 %, then 40 % and finally 80 % of the box volume), and visualised using GRASP [39]. For comparison, electrostatic calculations were also performed on the KcsA crystal structure. Pore dimensions were determined using the program Hole [40]. This also enabled a locus to be defined through the centre of the ion conduction pathway, along which the electrostatic potential (determined using Delphi) was analysed.

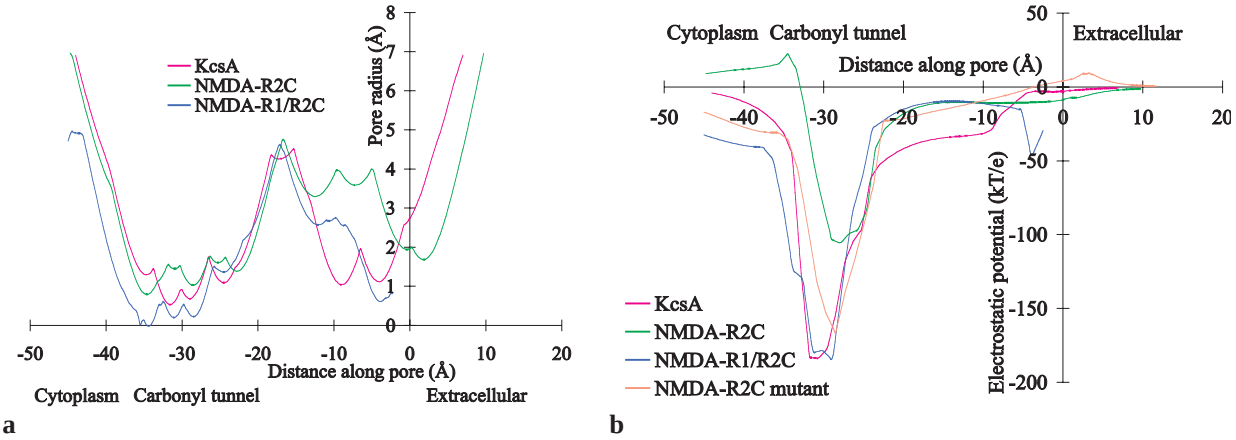

Figure 2 *Size of, and electrostatic potential along, ion conduction pathway of transmembrane domain. (***a***) Radius of the ion conduction pathway of the transmembrane domain as determined by Hole [40]. The selectivity filter in all structures has been aligned. (***b***) Electrostatic potential along the locus determined by Hole for the transmembrane region. "NMDA-R2C mutant" refers to homomeric (^{591}KGKKPGGP^{598}) NMDA-R2C (EEEEED). Note that the transmembrane topology of the KcsA channel is inverted in this Figure for comparison purposes, and 1* $k_BT/e \cong 2.2$ *kJ·mol^{-1} for a monovalent cation and 4.4 kJ mol^{-1} for a divalent cation.*

Agonist binding domain

The crystal structure of the S1S2 domain of GluR2 [22] (31% and 32 % sequence identity with NMDA-R2C and NMDAR1/R2C, respectively; PDB accession code 1GR2) was identified as the only suitable structural template for modelling the agonist binding domain of NMDA-R1 and NMDA-R2C (the bacterial periplasmic amino acid binding proteins, used previously, exhibit only ~ 20 % sequence identity with this domain). The amino acid sequences of the agonist binding domain of the NMDA receptors were aligned with that of the S1S2 domain of GluR2 using ClustalW and Cameleon, as before. The NMDA-R1 agonist binding domain was modelled with a glycine ligand, using protein-ligand distance restraints derived by analogy with the GluR2–kainate complex, and the NMDA-R2C agonist binding domain was modelled with a glutamate ligand (again with protein-ligand distance restraints derived by analogy with the GluR2–kainate complex), using the program Modeller. It should be noted that there is a certain degree of uncertainty in deriving these restraints, especially as the kainate-bound form of GluR2, unlike complexes of the lysine, arginine, ornithine binding protein-like structures, is thought not to have undergone full domain closure [22].

Ten models were generated for both the NMDA-R1–glycine and NMDA-R2C–glutamate complexes. In each case it was ensured that the consensus N-glycosylation sites were exposed to the solvent (and therefore to the incoming sugar molecule). Consistent stereochemical violations were removed manually by adjusting the alignment with Cameleon. The lowest energy model was selected and analysed, in particular verifying that those residues thought to contact agonist in NMDA-R1 (D372; [41]) and NMDA-R2 (R519, S690 and T691; [20,42]) were indeed in contact with agonist. An indication of the stereochemical quality of the models is given in Table 1. Although residues 412–454 (a loop towards the N-terminus of lobe 1) and 676-679 (a loop towards the N-terminus of lobe 2) from NMDA-R1, and the corresponding residues 420-456 and 675-680 from NMDA-R2C, were included in the models, these were not included in the analysis due to uncertainty in modelling these insertions.

Combining different modules

Following the construction of the models for the agonist binding domain and the channel domain, a more complete model of the NMDA receptor was produced guided by the available experimental data. The transmembrane domains were used as a starting point since they were built with the correct symmetry. Four copies of the ligand-binding domain were added to this using interactive molecular graphics (InsightII). The model of the agonist-binding domain was positioned empirically with respect to both the membrane and its symmetry related copies, so that **(1)** the consensus glycosylation sites were solvent accessible, **(2)** the agonist binding site was accessible, **(3)** the distance between the end of N-terminal section of the agonist-binding domain and M1 was in a reasonable range to allow the gap to be bridged by the 12 residues missing from our models in this region (corresponding to ^{545}KEIPRSTLDSFM^{555} in NMDA-R1), **(4)** the distance between the end of M3 and the start of the C-terminal section of the agonist-binding domain was also within a reasonable range to allow the gap to be bridged by the approximately seven residues missing from our models in this region (corresponding to ^{658}DRPEERI^{664} in NMDA-R1), and **(5)** the domain was as close to the pore as possible without overlapping sterically with its symmetry related copies. In the resulting orientation, the long axis of the agonist-binding domain was roughly parallel to the surface of the membrane. This positioning of the agonist-binding domain, although not a unique solution (due to the limited experimental data), is not inconsistent with the currently available data and is, in fact, constrained to a large extent by the experimental results.

Results and discussion

Transmembrane domain

Analysis of the size of the ion conduction pathway in the crystal structure of KcsA (using Hole; Figure 2a) suggests that this K^+ channel is in the closed form—the carbonyl tunnel (selectivity filter) has a minimum pore radius of ~ 0.5 Å, which is too small to allow K^+ ions (radius 1.33 Å) to pass. This in turn suggests that the models, which are based on KcsA, are also in the closed form. This does indeed appear to be the case. The minimum radius of "open" NMDA receptors is slightly below 3 Å, and the contribution of NMDA-R1 and NMDA-R2 subunits to pore size is thought to be asymmetric [43-45]. Analysis of the size of the ion conduction pathway of the models (using Hole; Figure 2a) shows that, in the vicinity of the selectivity filter, the size of the channels is much lower than expected, with pore radii as small as 0.8 Å and 0.0 Å in homomeric NMDA-R2C and heteromeric NMDA-R1/R2C, respectively. The Cα RMSD between the KcsA template structure and the models is 1.6 Å and 2.1 Å for NMDA-R2C and NMDA-R1/R2C, respectively. This corresponds roughly to the expected RMSD based on percentage amino acid sequence identity [46].

Additional evidence that the models are in the closed form comes from the conformation in the N-terminal region of what is denoted M1 in Figure 1. Experiments [47] suggest that, in the agonist free form, this region is α-helical, and changes conformation (*i.e.* the NMDA-R1 mutant Q556C becomes inaccessible to MTS reagents) when agonist is bound. Thus, the region around Gln 556 could form part of the M1 helix. Therefore the α-helix in M1, previously thought to start at Leu 562 (NMDA-R1) [21], now starts at Gln 556 (NMDA-R1). Other experiments [48] suggest that this region is involved in the desensitisation of NMDA receptors, serving as a dynamic link between ligand binding and channel

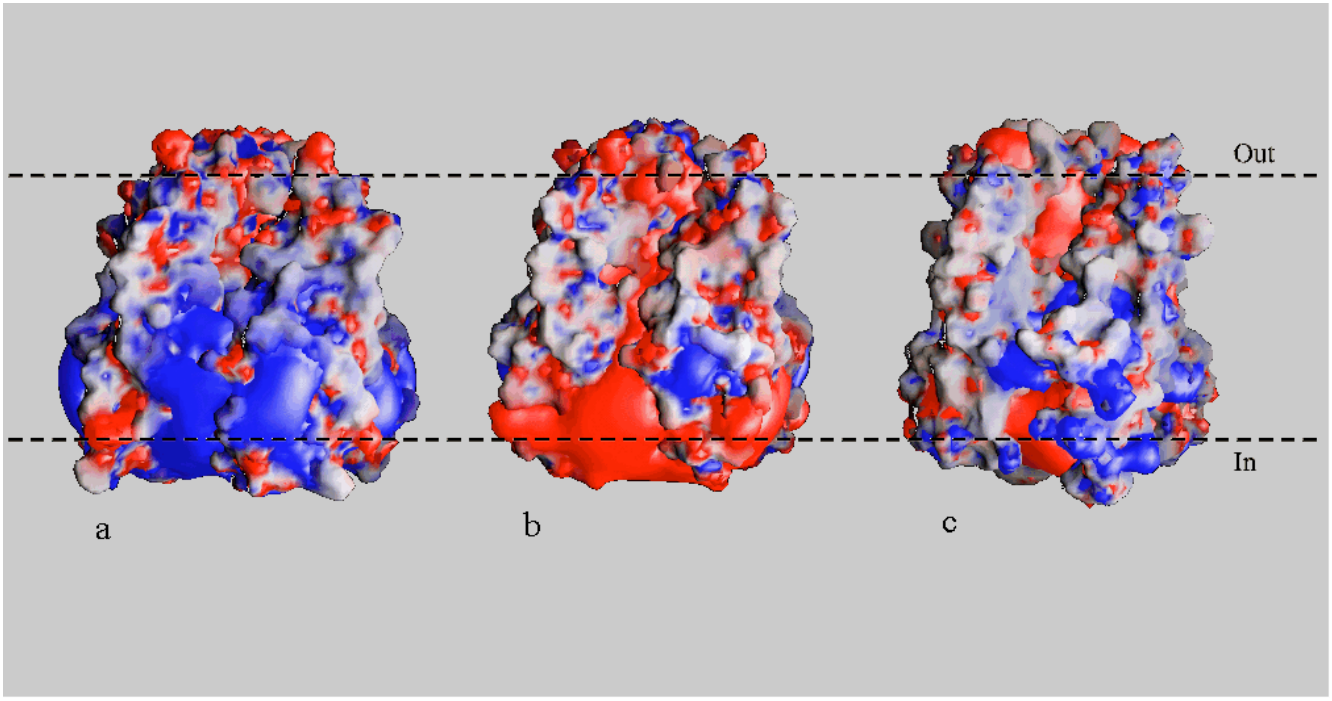

Figure 3 *Electrostatic potential surfaces for the transmembrane domain of* (**a**) *homomeric NMDA-R2C,* (**b**) *homomeric* (^{591}*KGKKPGGP*^{598}) *NMDA-R2C (EEEEED), and* (**c**) *heteromeric NMDA-R1/NMDA-R2C. Red corresponds to an electrostatic potential of* $\leq$ *-5* k_BT/e*, white an electrostatic potential of 0* k_BT/e *and blue an electrostatic potential of = +5* k_BT/e*. In addition to mapping the electrostatic potential onto the molecular surface, solid isopotential contours are shown at -5* k_BT/e *(red) and +5* k_BT/e *(blue). (Produced using GRASP [39])*

gating. Experiments [47] also suggest that the C-terminal portion of M3, contrary to our models, is not α-helical but that all the residues in this highly conserved region (^{648}TANLAAFLVLDR^{659} in NMDA-R1) are accessible to MTS reagents when mutated to cysteine. This suggests that either the symmetry has broken down in this region, or that there could be conformational dynamics that expose different residues at different instants of time, even with an α-helix. In turn, this could explain why we were unable to produce a conformation consistent with the simultaneous accessibility to the ion conduction pathway of so many continuous residues. Consequently, we **(1)** modelled M1 (as defined in

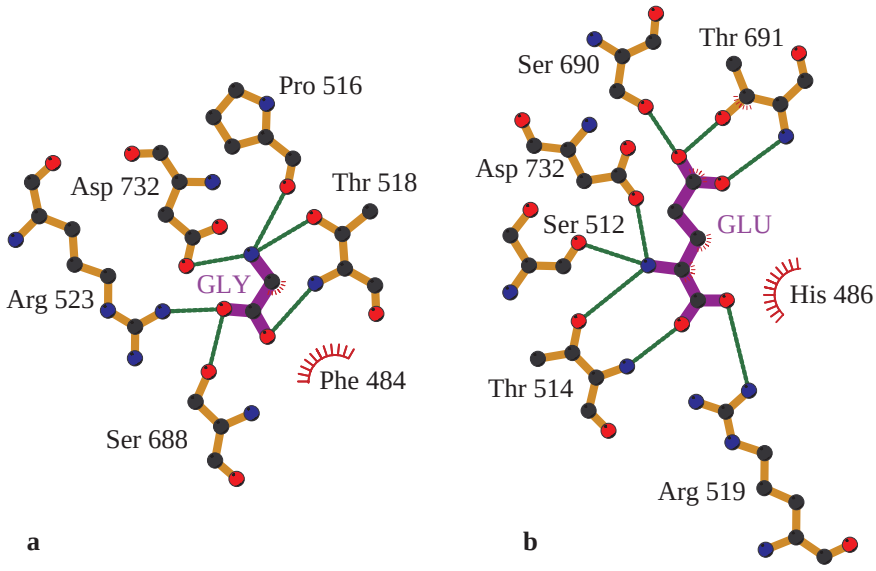

Figure 4 *Schematic representation of the modelled ligand binding site.* (**a**) *The glycine binding site in NMDA-R1.* (**b**) *The glutamate binding site in NMDA-R2C. Hydrogen bonds and charge—charge interactions are shown as green lines, hydrophobic interactions as red spoked arcs, carbon atoms as black balls, oxygen atoms as light red balls and nitrogen atoms as blue balls. (Produced using Ligplot [57])*

Figure 1) as completely α-helical, **(2)** modelled M3 as completely α-helical (as in the KcsA template), **(3)** excluded from our models those residues N-terminal of M1—^{552}DSFM^{555} (NMDA-R1) and ^{548}SAFL^{551} (NMDA-R2C), and **(4)** excluded from our models those residues C-terminal of M3—^{658}DRPEERI^{664} (NMDA-R1) and ^{657}EQYIDTV^{663} (NMDA-R2C).

Electrostatic calculations on homomeric NMDA-R2C and heteromeric NMDA-R1/R2C suggest that charged residues in the loop between the M1 and M2 segments could be important in channel activity. Determining the electrostatic potential along a locus that passes along the centre of the ion conduction pathway of the transmembrane domain reveals a significant difference at the cytoplasmic end of the channels—an electrostatic barrier, height ~ +20 k_BT/e (Figures 2a and 3a; where k_B is the Boltzmann constant, T the temperature in Kelvin and e the charge on an electron; for a monovalent cation 1 $k_BT/e \cong 2.2$ kJ mol^{-1} and for a divalent cation 1 $k_BT/e \cong 4.4$ kJ mol^{-1}) is present in NMDA-R2C. In contrast, the equivalent barrier height for NMDA-R1/R2C corresponds to a favourable interaction of ~ -50 k_BT/e (Figures 2a and 3c). However, switching residues ^{591}KGKKPGGP^{598} (*i.e.* a positively charged region) in the loop between M1 and M2 in NMDA-R2C for the corresponding residues from NMDA-R1, ^{594}EEEEED^{599} (*i.e.* a negatively charged region) changes what in wildtype NMDA-R2 is an electrostatic barrier into a favourable interaction (Figures 2b & 3b). Therefore, these electrostatic calculations suggest that a major reason why homomeric wildtype NMDA-R2C channels are non-functional is because the residues in the cytoplasmic M1–M2 loop are positively charged and therefore give rise to a large (electrostatic) energy barrier for cation to surmount. The homomeric NMDA-R2C mutant form is predicted to overcome the electrostatic barrier due to the introduction of a negative charge into the M1–M2 loop. This predicted pivotal role of electrostatics in channel function is consistent with the findings of other authors, *e.g.* [49,50].

It has been shown experimentally that mutating W606 to leucine in NMDA-R1 did not affect Mg^{2+} permeation [35], implying that this residue is not exposed to the ion conduction pathway. This is consistent with our NMDA-R1 model as this residue is buried in the protein, forming part of the

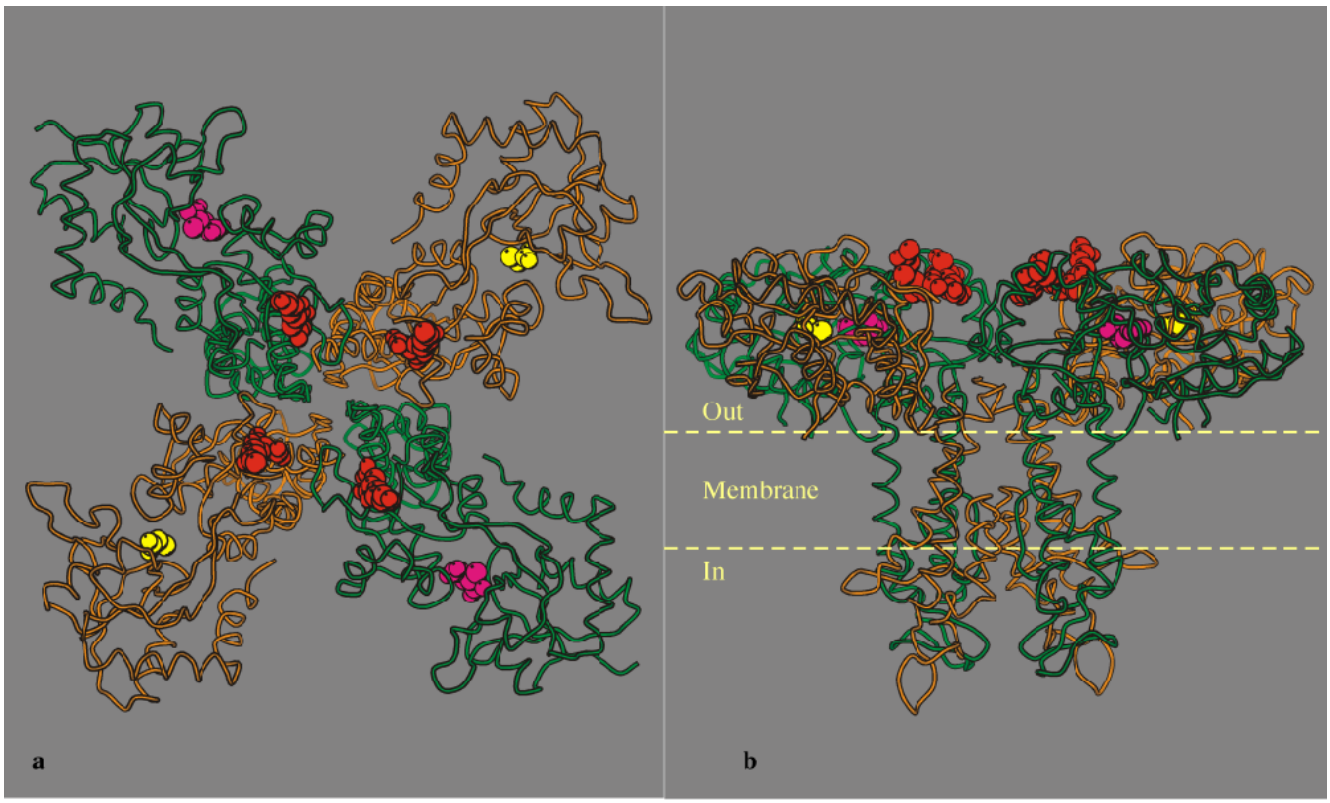

Figure 5 *Schematic representation of the tetrameric structure. The heteromeric NMDA-R1–glycine/NMDA-R2C–glutamate complex viewed from (***a***) outside the membrane and (***b***) along the membrane. NMDA-R1 subunits are shaded in orange and NMDA-R2C subunits in green, glycine ligand (NMDA-R1) and glutamate ligand (NMDA-R2C) are in yellow and magenta space filling representation, respectively, and the conserved acidic amino acid D669/D668 (NMDA-R1/NMDA-R2C, respectively) and the adjacent conserved acidic/polar residue N668/S667 are in red space filling representation. Residues 412–454 and 676-679 (NMDA-R1), and 420-456 (NMDA-R2C) and 675-680 are not shown due to uncertainty in modelling these insertions. (Figure produced using Molscript [58])*

Table 2 *The three positions within the binding site that contain different amino acid residues in NMDA-R1 and NMDA-R2C*

NMDA-R1	NMDA-R2C
Phe 484	His 486
Pro 516	Ser 512
Val 689	Thr 691

inter-subunit interface. When the equivalent mutation was carried out on NMDA-R2A and NMDA-R2B, permeation of extracellular magnesium increased, suggesting that this residue may line the pore. Since the NMDA-R2C is homologous to NMDA-R2A and NMDA-R2B, W607 in NMDA-R2C is perhaps expected to line the pore. This is inconsistent with our models—W607 does not line the pore, but lies behind the selectivity filter. However, the models suggest an alternative explanation—W607 appears to act as a "spacer" for the selectivity filter, and when this is mutated to a smaller residue it could allow the diameter of the selectivity filter to increase, thereby allowing the relatively large hydrated magnesium to permeate the channel.

Thus, despite the low sequence homology between the KcsA template and the NMDA receptors being modelled, the models for the transmembrane domain can be reconciled with experimental data. This supports the suggested similarity between the transmembrane domain of potassium channels and NMDA receptors [4,11].

Agonist-binding domain

Modelling of the agonist binding domain builds on the body of evidence that suggests the ligand binding domains of all glutamate subunits have a similar folding pattern, with ligand specificities probably accounted for by differences in amino acids (*e.g.* [1,3,21]). This may explain, at least in part, why the Cα RMSD between the GluR2 template structure and the models is 0.9 Å and 0.7 Å for NMDA-R2C and NMDA-R1, respectively—*i.e.* lower than that expected based on percentage amino acid sequence identity [46]. NMDA-R1 subunits are thought to bind glycine whereas the NMDA-R2 subfamily are thought to bind glutamate [18-20]. It has been suggested [20] that this difference in binding may arise from the presence of bulky aromatic sidechains in the α-amino binding region of NMDA-R1 subunits. Inspection of our models suggests that this is unlikely because these residues do not sterically hinder glutamate binding. An alternative suggestion [21] that a two amino acid insertion on NMDA-R1 (^{486}TQ^{487}, which is absent from NMDA-R2C) reduces the size of the NMDA-R1 binding site sufficiently to prevent glutamate from binding also appears unlikely because this proposed steric hindrance is absent from our current models. However, the NMDA-R1 and NMDA-R2C models do have three positions within the binding site that contain different amino acid residues (Table 2).

Phe 484 and His 486, in NMDA-R1 and NMDA-R2C respectively, are a similar distance (~3 Å) away from the glutamate ligand, and therefore not likely to affect ligand specificity (sterically). The sidechains of Pro 516 (NMDA-R1) and Ser 512 (NMDA-R2C) point away from the binding site and are therefore unlikely to explain any differences in ligand selectivity. However, ligand specificity is most likely explained by the sidechain hydroxyl of Thr 691 (NMDA-R2C) which forms an interaction (hydrogen bond) with the sidechain carboxyl group of glutamate ligand (Figure 4b). This hydroxyl-containing residue is conserved in other iGluRs (either Thr or Ser), but is absent on NMDA-R1 which contains a valine instead (Figure 4a). Furthermore, mutating the equivalent residue (T247) in GFKARβ [51] and chick kainate binding protein [52] abolished kainate binding, implying that this threonine is important in kainate binding. In our model of the GFKARβ–kainate complex [51], T247 forms an essential interaction with the carboxymethyl group of kainate, which is equivalent to Thr 691 (NMDA-R2C) interacting with the sidechain carboxyl of the glutamate. This is also suggested by the crystal structure of GluR2 [22]. As in our earlier studies [21,24,25], our models suggest that two amino acid positions (^{668}ND^{669} and ^{667}SD^{668} in NMDA-R1 and NMDA-R2C, respectively) may contribute charged residues to the outer opening of the channel (Figure 5). This is supported by the implication of these residues in voltage-dependent spermine block [53].

Experimental studies, *e.g.* [47,48,54], reinforce the belief that glutamate receptors are designed on a modular basis with the structural regions that link them serving as critical determinants of the coupling between ligand binding and channel gating. While in our models the ligand-binding domain corresponds to the agonist-bound form of the channel, the transmembrane domain on the whole apparently corresponds to the channel in a non-conducting form. Because of the difficulties in modelling the linkers between the extracellular domain and the channel domain, and the uncertainty concerning the orientation of the channel domain, insight into the structural basis of the propagation of the energy of agonist binding to channel opening and desensitisation will require further experimental evidence.

Conclusion

Our structural models of the pore-region of NMDA receptors suggest that electrostatics play an important part in channel activity. Positively charged residues in the cytoplasmic M1–M2 loop are suggested to be a major reason why NMDA-R2C subunits form a non-functional homomeric channel. Moreover, modelling suggests that changing the electrostatic properties of this loop changes the activity of the channel. In terms of ligand specificity, a single residue difference—removing the capacity to hydrogen bond—likely explains why NMDA-R1, unlike other iGluRs, is thought to bind glycine

in preference to glutamate. Thus, these new models have provided hypotheses that will be verified experimentally.

Acknowledgements KKC is a BBSRC Research Committee Special Student. We are grateful to Eric Gouaux for kindly supplying the coordinates of GluR2 prior to their release *via* the PDB. This work was supported in part by a grant from the National Science Foundation to REO (IBM-9974604).

References

1. Paas, Y. *Trends Neurosci.* **1998**, *21*, 117-125.
2. Monaghan, D. T.; Bridges, R. J.; Cotman, C. W. *Annu. Rev. Pharmacol. Toxicol.* **1989**, *29*, 365-402.
3. Dingledine, R.; Borges, K.; Bowie, D.; Traynelis, S. *Pharmacol. Rev.* **1999**, *51*, 7-61.
4. Wo, Z. G.; Oswald, R. E. *Trends Neurosciences* **1995**, *18*, 161-168.
5. Nakanishi, N.; Schneider, N. A.; Axel, R. *Neuron* **1990**, *5*, 569-581.
6. O'Hara, P. J.; Sheppard, P. O.; Thøgersen, H.; Venezia, D.; Haldeman, B. A.; McGrane, V.; Houamed, K. M.; Thomsen, C.; Gilbert, T. L.; Mulvihill, E. R. *Neuron* **1993**, *11*, 41-52.
7. Wo, Z. G.; Oswald, R. E. *Proc. Natl. Acad. Sci. USA* **1994**, *91*, 7154-7158.
8. Hollmann, M.; Heinemann, S. *Annu. Rev. Neurosci.* **1994**, *17*, 31-108.
9. Bennett, J. A.; Dingledine, R. *Neuron* **1995**, *14*, 373-384.
10. Wo, Z. G.; Oswald, R. E. *J. Biol. Chem.* **1995**, *270*, 2000-2009.
11. Wood, M. W.; van Dongen, H. M. A.; van Dongen, A. M. J. *Proc. Natl. Acad. Sci. USA* **1995**, *92*, 4882-4886.
12. Sprengel, R.; Suchanek, B.; Amico, C.; Brusa, R.; Burnashev, N.; Rozov, A.; Hvalby, O.; Jensen, V.; Paulsen, O.; Andersen, P.; Kim, J. J.; Thompson, R. F.; Sun, W.; Webster, L. C.; Grant, S. G.; Eilers, J.; Konnerth, A.; Li, J.; McNamara, J. O.; Seeburg, P. H. *Cell* **1998**, *92*, 279-289.
13. Kennedy, M. B. *Trends Neurosci* **1997**, *20*, 264-268.
14. Leonard, A. S.; Hell, J. W. *J. Biol. Chem.* **1997**, *272*, 12107-12115.
15. Moriyoshi, K.; Masu, M.; Ishii, T.; Shigemoto, R.; Mizuno, N.; Nakanishi, S. *Nature* **1991**, *354*, 31-37.
16. Soloviev, M. M.; Barnard, E. A. *J. Mol. Biol.* **1997**, *273*, 14-18.
17. McBain, C. J.; Mayer, M. L. *Physiol. Rev.* **1994**, *74*, 723-760.
18. Hirai, H.; Kirsch, J.; Laube, B.; Betz, H.; Kuhse, J. *Proc. Natl. Acad. Sci. USA* **1996**, *93*, 6031-6036.
19. Honer, M.; Benke, D.; Laube, B.; Kuhse, J.; Heckendorn, R.; Allgeier, H.; Angst, C.; Monyer, H.; Seeburg, P. H.; Betz, H.; Mohler, H. *J. Biol. Chem.* **1998**, *273*, 11158-11163.
20. Laube, B.; Hirai, H.; Sturgess, M.; Betz, H.; Kuhse, J. *Neuron* **1997**, *18*, 493-503.
21. Sutcliffe, M. J.; Smeeton, A. H.; Wo, Z. G.; Oswald, R. E. *J. Chem. Soc., Far. Disc.* **1998**, *111*, 259-272.
22. Armstrong, N.; Sun, Y.; Chen, G. Q.; Gouaux, E. *Science* **1998**, *395*, 913-917.
23. Doyle, D. A.; Cabral, J. M.; Pfuetzner, R. A.; Kuo, A. L.; Gulbis, J. M.; Cohen, S. L.; Chait, B. T.; MacKinnon, R. *Science* **1998**, *280*, 69-77.
24. Sutcliffe, M. J.; Smeeton, A. H.; Wo, Z. G.; Oswald, R. E. *Method. Enzymol.* **1998**, *293*, 589-620.
25. Sutcliffe, M. J.; Smeeton, A. H.; Wo, Z. G.; Oswald, R. E. *Biochem. Soc. Trans.* **1998**, *26*, 450-458.
26. Thompson, J. D.; Higgins, D. G.; Gibson, T. J. *Nucleic Acids Res.* **1994**, *22*, 4673-4680.
27. Bernstein, F. C.; Koetzle, T. F.; Williams, G. J. B.; Meyer, E. F.; Brice, M. D.; Rodgers, J. R.; Kennard, O.; Shimanovichi, T.; Tasumi, M. *J. Mol. Biol.* **1977**, *112*, 535-542.
28. Cuff, J. A.; Clamp, M.; Siddiqui, A. S.; Finaly, M.; Barton, G. J. *Bioinformatics* **1998**, *14*, 892-893.
29. Sali, A.; Blundell, T. L. *J. Mol. Biol.* **1993**, *234*, 779-815.
30. Kuner, T.; Wollmuth, L. P.; Karlin, A.; Seeburg, P. H.; Sakmann, B. *Neuron* **1996**, *17*, 343-352.
31. Rosenmund, C.; Stern-Bach, Y.; Stevens, C. F. *Science* **1998**, *280*, 1596-1599.
32. Mano, I.; Teichberg, V. I. *Neuroreport* **1998**, *9*, 327-331.
33. Laube, B.; Kuhse, J.; Betz, H. *J. Neurosci.* **1998**, *18*, 2954-2961.
34. Premkumar, L. S.; Auerbach, A. *J. Gen. Physiol.* **1997**, *110*, 485-502.
35. Williams, K.; Pahk, A. J.; Kashiwagi, K.; Masuko, T.; Nguyen, N. D.; Igarashi, K. *Mol. Pharmacol.* **1998**, *53*, 933-941.
36. Kashiwagi, K.; Pahk, A. J.; Masuko, T.; Igarashi, K.; Williams, K. *Mol. Pharmacol.* **1997**, *52*, 701-713.
37. Chao, J.; Seiler, N.; Renault, J.; Kashiwagi, K.; Masuko, T.; Igarashi, K.; Williams, K. *Mol. Pharmacol.* **1997**, *51*, 861-871.
38. Nicholls, A.; Honig, B. *J. Comput. Chem.* **1991**, *12*, 435-445.
39. Nicholls, A.; Sharp, K.; Honig, B. *Proteins* **1991**, *11*, 281-296.
40. Smart, O. S.; Goodfellow, J. M.; Wallace, B. A. *Biophys. J.* **1993**, *65*, 2455-2460.
41. Williams, K. *Neurosci. Lett.* **1996**, *215*, 9-12.
42. Anson, L. C.; Chen, P. E.; Wyllie, D. J. A.; Colquhoun, D.; Schoepfer, R. *J. Neurosci.* **1998**, *18*, 581-589.
43. Zarei, M. M.; Dani, J. A. *J. Neurosci.* **1995**, *15*, 1446-1454.
44. Villarroel, A.; Burnashev, N.; Sakmann, B. *Biophys. J.* **1995**, *68*, 866-875.
45. Wollmuth, L. P.; Kuner, T.; Seeburg, P. H.; Sakmann, B. *J. Physiol., (London)* **1996**, *491*, 779-797.
46. Chothia, C.; Lesk, A. M. *Embo J.* **1986**, *5*, 823-826.
47. Beck, C.; Wollmuth, L. P.; Seeburg, P. H.; Sakmann, B.; Kuner, T. *Neuron* **1999**, *22*, 559-570.
48. Krupp, J. J.; Vissel, B.; Heinemann, S. F.; Westbrook, G. L. *Neuron* **1998**, *20*, 317-327.
49. Eisenberg, R. S. *J. Membr. Biol.* **1996**, *150*, 1-25.

50. Roux, B.; MacKinnon, R. *Science* **1999**, *285*, 100-102.
51. Wo, Z. G.; Chohan, K. K.; Chen, H.; Sutcliffe, M. J.; Oswald, R. E. *J. Biol. Chem.* **1999**, *274*, 37210-37218.
52. Paas, Y.; Eisenstein, M.; Medevielle, F.; Teichberg, V. I.; Devillers-Thiery, A. *Neuron* **1996**, *17*, 979-990.
53. Kashiwagi, K.; Fukuchi, J. I.; Chao, J.; Igarashi, K.; Williams, I. *Mol. Pharmacol.* **1996**, *49*, 1131-1141.
54. Villarroel, A.; Regalado, M. P.; Lerm, J. *Neuron* **1998**, *20*, 329-339.
55. Laskowski, R. A.; MacArthur, M. W.; Moss, D. S.; Thornton, J. M. *J. Appl. Cryst.* **1993**, *26*, 283-291.
56. Barton, G. J. *Protein Eng.* **1993**, *6*, 37-40.
57. Wallace, A. C.; Laskowski, R. A.; Thornton, J. M. *Protein Eng.* **1995**, *8*, 127-134.
58. Kraulis, P. J. *J. Appl. Crystallogr.* **1991**, *24*, 946-950.